energies

MDPI

Article

Design and Optimization of a Gorlov-Type Hydrokinetic Turbine Array for Energy Generation Using Response Surface Methodology

Andrés Chalaca [1], Laura Velásquez [1], Ainhoa Rubio-Clemente [1,2,*] and Edwin Chica [1,*]

[1] Grupo de Energía Alternativa, Facultad de Ingeniería, Universidad de Antioquia, Calle 70 No. 52-21, Medellín 050010, Colombia; andres.chalaca@udea.edu.co (A.C.); lisabel.velasquez@udea.edu.co (L.V.)
[2] Escuela Ambiental, Facultad de Ingeniería, Universidad de Antioquia, Calle 70 No. 52-21, Medellín 050010, Colombia
* Correspondence: ainhoa.rubioc@udea.edu.co (A.R.-C.); edwin.chica@udea.edu.co (E.C.); Tel.: +57-6042195550 (E.C.)

Abstract: Hydrokinetic arrays, or farms, offer a promising solution to the global energy crisis by enabling cost-effective and environmentally friendly energy generation in locations with water flows. This paper presents research focused on the design and optimization of a Gorlov-type vertical-axis hydrokinetic turbine array for power generation. The study involved (i) numerical simulations using computational fluid dynamics (CFD) software with the six degrees of freedom (6DoF) tool, (ii) optimization techniques such as response surface methodology, and (iii) experimental testing in natural environments. The objective was to develop an efficient system with low manufacturing and maintenance costs. A key finding was that the separation distance between rotors, both along and across the fluid flow, is a critical parameter in designing hydrokinetic arrays. For this study, a triangular array configuration, termed Triframe, was used, consisting of three Gorlov-type turbines with four blades each. The optimization process led to separation distances based on the diameter (D) of the turbines, with 15.9672D along the fluid flow (X) and 4.15719D across the flow (Y). Finally, an experimental scale model of the hydrokinetic array was successfully constructed and characterized, demonstrating the effectiveness of the optimization process described in this study.

Keywords: hydrokinetic array; hydrokinetic farm; Gorlov-type hydrokinetic turbine; energy generation; renewable energy; response surface methodology

check for updates

Citation: Chalaca, A.; Velásquez, L.; Rubio-Clemente, A.; Chica, E. Design and Optimization of a Gorlov-Type Hydrokinetic Turbine Array for Energy Generation Using Response Surface Methodology. *Energies* **2024**, *17*, 4870. https://doi.org/10.3390/en17194870

Academic Editor: Ahmed Abu-Siada

Received: 29 August 2024
Revised: 19 September 2024
Accepted: 26 September 2024
Published: 28 September 2024

Copyright: © 2024 by the authors. Licensee MDPI, Basel, Switzerland. This article is an open access article distributed under the terms and conditions of the Creative Commons Attribution (CC BY) license (https://creativecommons.org/licenses/by/4.0/).

1. Introduction

In recent decades, the population growth and socio-economic development of countries have led to a worldwide trend characterized by increasing energy demand, primarily dominated by fossil fuels (natural gas, oil, coal) [1,2]. However, the global energy dependence on fossil fuels has adverse effects on the environment, including global warming associated with the excessive emission of greenhouse gases (GHGs) [3]. Structural changes in how energy is produced and consumed are necessary to meet the current high energy demand and mitigate the increase in emissions (GHGs) that detrimentally impact climatic conditions. Renewable energies are regarded as an opportunity for a global energy transition from fossil fuels to clean and sustainable energy sources (hydropower, wind, photovoltaic solar, geothermal, biomass). Therefore, governments, in collaboration with international organizations, have begun to formulate decisive actions in the field of energy and climate change, aiming to meet current demands without jeopardizing future generations [4]. Energy production from renewable sources offers various options, such as hydropower. This form of energy is based on the transformation of hydraulic energy into electricity and consists of potential and kinetic energy. Potential energy can be extracted through dams or water flows at a certain height, while kinetic energy is related to water

velocity [4]. The devices that convert potential energy into mechanical and electrical energy through an electrical generator are called hydraulic turbines, with the most well-known being the Pelton, Kaplan, and Francis turbines [5]. Additionally, kinetic energy has a less explored hydropower potential and can be harnessed by unconventional hydraulic turbines such as hydrokinetic turbines (HKT) in natural water currents found in oceans, rivers, and low-flow canals, where conventional turbines are less viable [6]. Compared to a conventional hydropower plant, the energy produced by HKT is not very high; however, hydrokinetic technology has gained significant momentum. Unlike conventional hydropower plants, there is no need for the construction of civil works (dams, reservoirs, canals, and load tunnels), which have a considerable economic cost and generate significant environmental and social impact in their implementation [7–9].

There are different types of HKT, and a general classification is based on the orientation of the turbine's axis of rotation and the flow direction, resulting in the following two types: (a) axial flow turbines (HAHT) and (b) cross-flow turbines (VAHT) [7]. In a HAHT, the turbine's axis of rotation is generally aligned with the flow direction. In contrast, in a VAHT, the axis of rotation is orthogonal to the flow direction. VAHTs have advantages in terms of the implementation and use of conventional turbines, such as the ability to self-start in shallow waters, low manufacturing costs, and ease of operation and maintenance, as they mainly consist of a generator group installed on the riverbed [7,10]. Among the various types of VAHT rotors, the following three are primarily distinguished: Darrieus and its variations, Savonius, and Gorlov. The Gorlov-type HKT stands out in its class due to its ability to self-start in low-speed currents and its better torque stability, increasing its efficiency and reducing intermittency in the generation of electrical energy [11].

An alternative for harnessing hydropower potential through hydrokinetic technology is provided by systems known as hydrokinetic arrays or farms. These systems are equipped with a certain number of turbines, which can be VAHT or HAHT [12], and are considered a promising means to generate energy economically and ecologically in almost any location with water flows, allowing for a reduction in energy dependence on fossil fuels in a context of increasing resource scarcity [7]. However, the implementation of hydrokinetic arrays or farms in rivers faces pending tasks, such as the development of methodologies to define the location and arrangement of the turbines within the array. The passage of fluid through the turbine generates a downstream turbulence region known as the fluid wake; thus, the spacing between turbines plays a significant role [13]. The wake length and the available space for installation will influence the number of turbines to be installed, the amount of captured energy, and, in turn, the overall viability of the hydrokinetic system for energy production.

There are specific cases around the world where hydrokinetic farms of various capacities have been implemented, most of them in the United States and Asia: a power unit consisting of six HAHT turbines in the city of Hastings, Minnesota, USA, with a capacity of 100 kW [14]; an energy unit consisting of two HKT turbines in the Chilla canal, India, with a capacity of 50 kW [15]. In South America, there are no reports of studies or the developments of Gorlov-type HKT arrays. Research in Brazil focuses on the implementation of HAHT and simplified turbines using the actuator disk model [13].

The available information on the specialized design, optimization, and implementation of hydrokinetic arrays or farms is somewhat scattered and primarily focused on very specific cases: (a) systems equipped with a single turbine and (b) arrays or farms equipped with HAHT, based on wind farm models [16]. This study stands out as a pioneering effort, as it specifically addresses the design and optimization of a Gorlov-type VAHT array, an area that has not been extensively explored before.

In recent studies, Cacciali et al. [17] introduced a multi-array tool for evaluating turbine arrays in mild slope hydropower canals, providing reliable power output estimates by modeling hydraulic transitions. The tool integrates a 1-D channel model with a Double Multiple Streamtube code and wake sub-models to optimize array power. Results show

that power output scales linearly for up to five arrays, while water depth variation follows a power law from the downstream array towards upstream, independent of plant size.

Okulov et al. [18] presented an experiment on the interference of multiple horizontal-axis hydro turbines arranged in a line array. This was the first time turbine output has been optimized by adjusting operating conditions. The results show that power decreases significantly for the second turbine but then increases and stabilizes for the third and subsequent turbines, contradicting early theoretical predictions of continual performance decline. This stabilization suggests that line arrays of hydro turbines, similar to wind farms, could be effectively used in rivers. The study highlights the benefits of line arrays for river power extraction, such as reduced environmental impact and continued navigation, but emphasizes the need for further research on power stabilization, array configurations, and blockage effects.

Multiple hydrokinetic turbines in three array configurations were analyzed by Riglin et al. [19], using Reynolds-averaged Navier–Stokes equations. The simulations were performed on existing turbines operating at an optimal power coefficient of 0.43. Mechanical power was predicted for adjacent turbines at various lateral separations, and a two-by-two turbine array was studied to simulate a hydro-farm. At a lateral separation of $0.5D$, turbines achieved 86% of the peak power of a single turbine. Interaction effects were minimal at separations greater than $2.5D$. However, downstream turbines experienced significant performance reductions within $6D$ longitudinal spacing, performing around 20% or less compared to a single turbine. These results align with experimental findings.

dos Santos et al. [13] introduced a methodology for assessing the length of hydrokinetic rotor wakes in natural channels using computational fluid dynamics techniques and the actuator disk model. Applied to a segment of the Brazilian Amazon River with real field data on velocity, curvature, and geometry, the wake length was found to be between seven and nine diameters, depending on the turbine's operating point. Additionally, an evaluation of a three-turbine hydrokinetic setup yielded an electrical power output of 18.3 kW.

The goal of this research work is to advance knowledge in the field of renewable energy by proposing a novel approach for the design and optimization of Gorlov-type VAHT arrays for energy generation. This includes utilizing numerical simulations in computational fluid dynamics (CFD) software, conducting experimental tests, and employing a response surface methodology to achieve an efficient system with low manufacturing and maintenance costs.

This study represents a significant innovation, particularly concerning Gorlov-type hydrokinetic arrays. The combination of advanced simulation techniques and experimental validation ensures that the findings are not only theoretically robust but also practically applicable. By addressing a gap in the current research landscape, this study provides valuable insights for future developments in hydrokinetic energy and could guide large-scale implementations in regions with untapped hydrokinetic potential. The innovative approach and focus on optimization contribute to the growing body of knowledge in renewable energy technologies, positioning this research as a crucial step toward sustainable energy solutions.

2. Methods and Materials

2.1. Hydrokinetic Turbines

For the design of HKT, theoretically, hydrokinetic energy can be expressed using Equation (1), where the theoretical hydrokinetic power P_{HKT} is proportional to the rotor area A, the cube of the flow velocity U^3 and the fluid density ρ. Hence, a larger rotor can generate more power, and even a small increase in flow velocity significantly increases the generated power. However, the technically extracted power is much lower in comparison to the theoretical hydrokinetic power and depends on the system used to harness the kinetic energy of the fluid flow. An HKT captures only a fraction of the kinetic energy available in the fluid stream. This fraction is known as the power coefficient C_p, and it can be expressed using Equation (2). The power captured by the turbine P_{rot} is equal to the product of the torque T produced on the rotor axis and the angular velocity ω, as expressed

in Equation (3). It is important to mention that HKTs share operational principles with wind turbines and have a theoretical reference when evaluating the utilization of a fluid flow's potential, known as the Betz limit [20]. In addition to the power coefficient C_p, it is necessary to define two dimensionless quantities: the tip-speed ratio TSR, which relates the product of the turbine's angular velocity ω and its radius R to the fluid flow velocity, as expressed in Equation (4). Equation (5) establishes the aspect ratio AR as the relationship between the turbine's height H and its diameter D.

$$P_{HKT} = \frac{1}{2}\rho A U^3 \tag{1}$$

$$P_{rot} = C_p P_{HKT} \tag{2}$$

$$P_{rot} = T\omega \tag{3}$$

$$TSR = \frac{\omega R}{U} \tag{4}$$

$$AR = \frac{H}{D} \tag{5}$$

2.2. Gorlov-Type VAHT

Among vertical-axis hydrokinetic turbines (VAHT), the Gorlov-type turbine stands out due to its ability to self-start in low-speed currents and the better stability in its generated torque. The Gorlov turbine was patented by Professor Alexander Gorlov at Northeastern University as an evolution of the Darrieus H-type turbines. It retains the aerodynamic sections shaping the rotor blades but adds a helical angle, transitioning from straight blades to helical ones. This feature allows for more efficient utilization of the fluid flow, increasing the contact surface that facilitates the turbine's rotation. As a result, the turbine operates with less vibration than its counterparts, reducing fluctuations in torque measurement and the power coefficient. The turbine's rotation is independent of the flow direction and can operate in any orientation perpendicular to the flow. It is specially designed to work with low-current intensities and can be implemented in rivers, canals, and tidal power generation systems [21]. This is a compact machine that is easy to handle, has low manufacturing costs, and exhibits minimal mechanical vibration [22].

The turbine used for this study was a scaled model of a Gorlov-type VAHT with four blades. The geometry and its characteristics are shown in Figure 1 and Table 1.

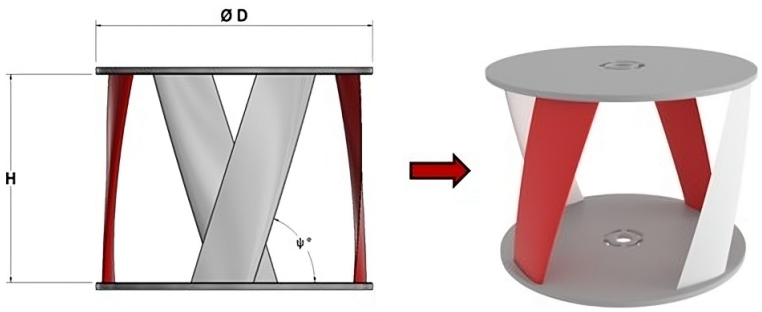


Figure 1. Geometric characteristics and CAD model of the Gorlov-type VAHT.

Table 1. Geometric parameters of the Gorlov-type VAHT.

Parameter	Value
Diameter (D)	160 mm
Height (H)	120 mm
Aspect ratio (H/D)	0.75

Table 1. *Cont.*

Parameter	Value
Helix angle (ψ)	70°
Number of blades	4
Hydrofoil	NACA 0015
Chord length (C)	40 mm
Angle of attack (α)	9°

2.3. Hydrokinetic Arrays

There are different types of turbine arrays (linear, triangular, matrix, staggered) reported in the literature that can be applied for the extraction of hydrokinetic and tidal energy [23,24]. According to the existing literature, the energy production efficiency from hydrokinetic arrays varies depending on the type of turbine used and its position within the array. The spacing between turbines plays a vital role in mitigating the turbulent intensity of the wake produced by the turbines, which affects the downstream rotor performance. Staggered and triangular arrays outperform other designs, with the highest rates of flow velocity recovery observed in the triangular configuration, characterizing it as an interesting model for the planning of hydrokinetic farms [15,25,26]. The characterization of wakes is limited, and the complexity of estimating the wake and the many uncertainties in modeling this phenomenon has been noted [24,27]. Most studies on hydrokinetic wakes use Reynolds-averaged Navier–Stokes RANS–Shear Stress Transport SST tools, such as turbulence modeling approaches. It is important to highlight that wake characterization involves numerous parameters, and the wake dissipation length significantly varies among the literature works [12,26,28]. The transient approach is the most recommended for wake modeling because it can provide a more expressive and realistic wake behavior [15,29].

Table 2 presents the findings and authors whose studies report and suggest the magnitude of the distances between turbines to be considered for the design of hydrokinetic arrays, based on the turbine diameter D.

Table 2. Spacing in directions (X, Y) between hydrokinetic turbines reported in the literature.

Author	Spacing in X	Spacing in Y
González-Gorbeña et al. [27]	$10D \leq X \leq 20D$	$2D \leq X \leq 4D$
Riglin et al. [19]	$X \geq 7D$	$Y \geq 3D$
Patel et al. [12]	$X \geq 6D$	$0.5D \leq X \leq 2.5D$
Birjandi and Bibeau [28]	$X \geq 1.5D$	-
Chawdhary et al. [26]	$X = 2D$	$Y = 3D$
Nag and Sarkar [15]	$X = 4D$	$Y = 4D$
dos Santos et al. [13]	$X \geq 9D$	-

For this work, a triangular array was considered, consisting of three rotors, similar to the studies [26,29], which report various advantages of this type of triangular configuration, also known as the TriFrame. In this configuration, two rotors interact with the fluid current simultaneously, and a third rotor is located downstream. This arrangement aims to limit interference from the wake generated by the first two rotors. A coordinate system (X, Y) was established to represent design variables, as seen in the schematic of Figure 2. The distance between the channel edges and the rotors was determined according to the study reported by [27] and was considered in the computational domain for numerical simulations.

The independent factors to consider in the hydrokinetic array design were as follows:

- Downstream spacing between rotors (X): the distance between rotor centers as a function of the diameter D, measured in the direction of the fluid current flow.
- Horizontal spacing between rotors (Y): the distance between rotor centers as a function of the diameter D, measured across the fluid current.

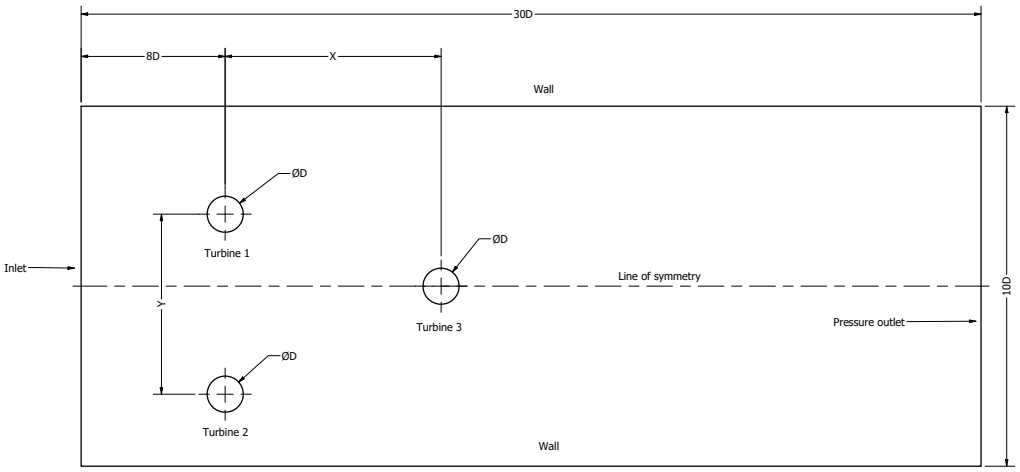


Figure 2. Schematic of the parametric model for hydrokinetic array design.

2.4. Response Surface Methodology (RSM) and the Design of Experiments (DOE)

Response surface methodology (RSM) has been employed to optimize the efficiency of turbomachinery by exploring the relationship between independent variables and their combined effect on the studied response [30–32]. In the optimization process of hydrokinetic turbines, it has been observed that working in conjunction with the design of experiments (DOE) is necessary. DOE allows the evaluation of the process or product conditions using a minimal number of tests and the subsequent construction of a mathematical model that can adequately fit the results of the studied physical phenomenon. The application of RSM allows for an exploration of the response region, from which the path or trajectory toward the optimal combination of variables can be defined to achieve the desired result [33]. Various DOEs allow the analysis of the effect or impact of multiple factors on a response variable. In many cases, it is necessary to assume the relationship between the response and the factor. If a linear result is expected, defining only 2 levels (2^k factorial design, k factors at 2 levels) will suffice. However, this approach may risk neglecting the quadratic effect. To avoid this, 3 levels should be defined (3^k factorial design, k factors at 3 levels) to analyze the curvature, linear effects, and interactions [33]. However, the 3^k factorial design is not the only way to model quadratic effects, as it requires many experimental units when testing the effect of more than 4 factors. In such cases, central composite designs or Box–Behnken designs are commonly used [33]. In the specific case of the hydrokinetic array equipped with Gorlov-type VAHT, two factors were defined related to the spacing between rotors and as a function of the diameter D: (X) and (Y). The response variable was defined as the sum of the power generated by each rotor, resulting in the total power of the array (P). To model the quadratic relationship between factors (X) and (Y), it was determined that the 3^k factorial design corresponded to the most suitable design of experiments. According to the levels of the factors reported in Table 2, used to evaluate the effect of rotor spacing on the power generated by the hydrokinetic array, two factors were defined with three levels of variation: (i) low, (ii) medium, and (iii) high, represented as −1, 0, and 1, resulting in nine treatments or experimental units. Table 3 presents the values for each level, and Table 4 presents the factor combinations summarized into nine experimental units for subsequent analysis through numerical simulations.

Table 3. Independent factors and levels used for the optimization process of the hydrokinetic array.

Independent Factor	Values		
Standard levels	−1	0	1
$X(D)$	6	11	16
$Y(D)$	2	4	6

Table 4. Experimental units for analysis through numerical simulations.

Experimental Unit	$X(D)$	$Y(D)$
1	16	2
2	11	4
3	11	2
4	16	6
5	11	6
6	6	6
7	16	4
8	6	4
9	6	2

2.5. Numerical Simulation Setup

The process of numerical simulation begins by modeling the computational domain. For this, dimensional characteristics used in various related studies were considered [34,35]. Subsequently, a 3D computational domain was created in CAD software to simulate the nine treatments or experimental units resulting from the DOE. The computational domain consisted of two bodies. The first body represented the flow away from and external to the rotors, similar to a water channel, referred to as the stationary domain. The second type of body consisted of a cylinder enclosing each of the three rotors, referred to as the rotational domain, which is dynamic. Boundary conditions were assigned, including velocity inlets, outlet pressure, walls, and interfaces. The computational domain model is shown in Figure 3.

Once the computational domain was determined and modeled, meshing was performed. Since it is a 3D computational domain composed of two types of bodies, it was decided to separate each body and create a mesh for each. This meshing process was carried out using the Fluent-Meshing tool in the ANSYS software 2021 R1. The mesh used was a combination of an unstructured polyhedral type near the hydrofoil and a poly-hexcore type further away from the blades. According to various authors, polyhedral meshes have the advantage of facilitating the use of unstructured meshes near walls with complex geometries. Furthermore, their use considerably reduces the number of elements, thus decreasing computation time and notably improving convergence [36,37].

The results of the mesh can be visualized in Figure 4, which depicts an isometric cutaway view of the computational domain of the hydrokinetic array equipped with four-blade Gorlov rotors. The mesh was refined around the rotor blades to capture the fluid–surface interaction phenomena in detail.

The simulation conditions for the various hydrokinetic array configurations are summarized below:

The region called “interface” was merged for both domains (stationary and rotational) to allow for an exchange of information regarding pressure and velocity fields between the meshes. The external domain walls were set to a no-slip wall boundary condition, which was also applied to the turbine blades. The simulation was conducted in a transient regime, with an inlet velocity set at 1 m/s. A turbulence intensity of 5% and a turbulent viscosity ratio of 10 were assumed, as seen in the ANSYS Fluent software’s turbomachinery simulation examples [38]. The pressure outlet boundary condition was set with a manometric pressure of 0 Pa. The working fluid was considered to be liquid water with a constant density of 997 kg/m^3, equivalent to a theoretical hydrokinetic power (P_{HKT}) of 9.57 W.

The chosen turbulence model for these simulations was k-ω SST due to its ability to predict adverse pressure gradients near complex geometry walls and model the wake accurately in regions farther from the wall [39]. This allows for the precise prediction of turbine performance and wake behavior. The SIMPLE solution method was used, and the transient formulation was maintained as the default first order. To capture the angular movement of the rotors, the six degrees of freedom (6 DoF) solver available in ANSYS

Fluent was utilized. This solver uses the forces and moments of the object to calculate the translation and angular movement of the object's center of gravity [38].

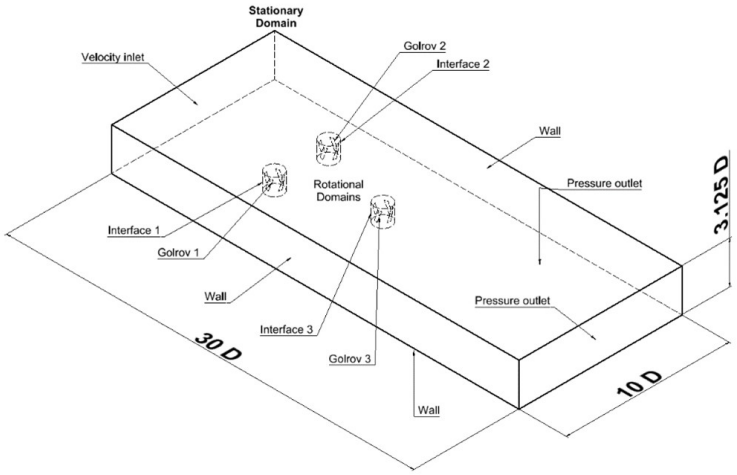


Figure 3. Computational domain for the hydrokinetic array simulation.

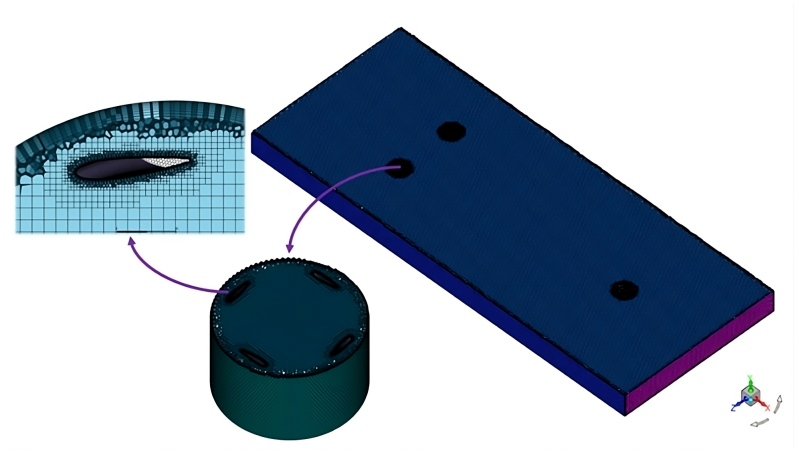


Figure 4. Mesh for the hydrokinetic array simulation.

The 6 DoF tool in CFD simulations allows us to model the full motion of objects in a fluid by considering their ability to move in six independent directions. These include translational movements along the x, y, and z axes and rotational movements around these axes [40–42]. This method is particularly useful when simulating the interaction between fluid dynamics and the physical movement of objects, such as turbines, boats, or drones. In CFD, the 6 DoF tool calculates the forces and moments acting on the object based on the fluid's flow, pressure, and velocity fields in real time, and predicts sequentially the angular positions according to the turbines mass properties (mass and moment of inertia) [43]. After configuring and running the simulation, the 6-DoF model accelerated due to the interaction between the fluid and turbine walls, reaching a stable maximum angular velocity (ω). A preload was then applied, causing the turbine to slow down until it stopped (0 rad/s). The data collected during this process were used to plot the C_p vs. TSR curve.

The "One-DOF-rotation" option was activated, and a mesh deformation method called "smoothing-diffusion" was employed. The angular movement of the Gorlov-type rotor is considered rigid-body movement, with the internal walls moving relative to one another. The movement of the walls must be specified through the reference axes of the rigid body in question, the direction of angular momentum, the mass, and its inertia. During the simulations, it was observed that there is a very high acceleration during the initial moments of rotor rotation when the torque on the turbine is highest because it remains fixed, allowing the flow field to reach a steady state. Afterward, the turbine's acceleration surpasses the

torque imposed by the fluid, causing a brief deceleration. Once the turbine's rotation and the flow field start rotating together, they reach steady-state operation with the turbine rotating at a uniform angular velocity, known as the free-wheeling speed. At this point, the angular momentum is minimal because the turbine shaft experiences no braking moments. It is possible to assign braking loads to the shaft, which is expected to gradually decrease the turbine's rotation speed until it reaches a minimum point [44,45]. For this case, the braking loads ranged between 0.02 and 0.05 Nm. This procedure was followed to plot the characteristic curve of each rotor in terms of C_p and TSR and to calculate the power of the rotors that make up the hydrokinetic array.

Mesh independence and temporal independence were assessed to ensure that the results obtained with different meshes did not significantly deviate from each other. The optimal mesh size was determined using the Grid Convergence Index (GCI) method, which is based on Richardson extrapolation and provides an estimate of the exact solution [46]. The power of the entire array (P), defined as the sum of the power generated by each rotor, was the standard of measurement for analyzing the variation in simulation results. The number of elements used for mesh independence testing was divided into three cases: fine mesh, medium mesh, and coarse mesh, with 8.9, 4.4, and 2.2 million elements, respectively. A temporal independence study was also conducted to determine the most suitable time step for simulations. Time steps of 0.002, 0.005, and 0.008 s were used for this test. Figure 5 represents the results obtained for the independence tests and Richardson extrapolation solutions. After the Richardson extrapolation analysis, the medium mesh and a time step of 0.008 s were selected. These choices exhibited deviations close to 2% for the Richardson extrapolation solution and reduced the computation time.

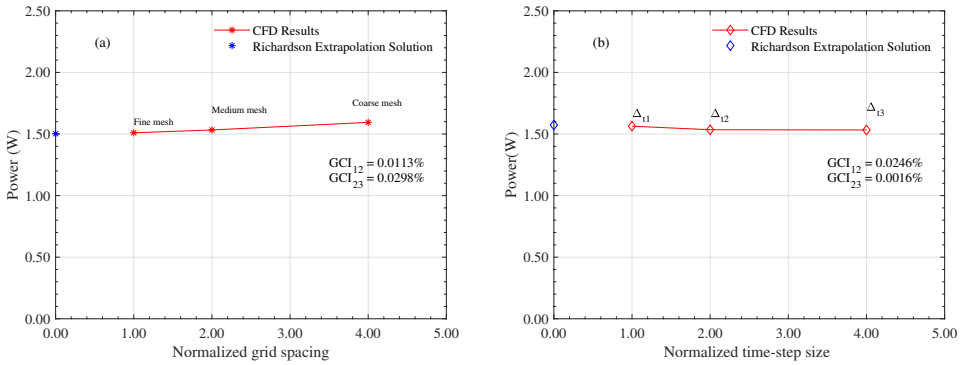


Figure 5. Results of mesh and temporal independence studies. (**a**) Mesh independence test. (**b**) Temporal independence test.

2.6. Experimental Test

2.6.1. Manufacturing of Scale Models of Vertical-Axis Hydrokinetic Gorlov Turbines

For this work, the additive manufacturing process (3D printing) was chosen due to its technical availability and its advantages, such as the ability to produce parts with complex geometries, good surface finish, and high strength [47]. The scale model of the vertical-axis hydrokinetic Gorlov turbine was divided into three manufacturable parts: lower support plates, upper support plates, and the turbine blades. This division was made because 3D printing allows for the creation of complex geometries, but printing the entire model in a single piece could result in issues with surface finish. After defining the manufacturing process for the scale models of the Gorlov turbines, the next aspect to consider was the choice of material for printing the models. Based on information found in the literature, PLA was selected as the material for manufacturing the blades of the hydrokinetic Gorlov turbine. PLA (polylactic acid) is a biodegradable thermoplastic material derived from renewable resources such as corn, sugarcane, and other natural starches. It is widely used in 3D printing due to its ease of use, low cost, and ability to produce parts with good surface quality [47–49].

With the defined manufacturing process and material, and taking into account the parameters provided by the manufacturers for printing PLA, three rotors were replicated using the same 3D printing techniques, as shown in Figure 6. The recommended printing parameters for PLA include a nozzle temperature range of 180 °C to 220 °C, a bed temperature set between 50 °C and 60 °C, and a printing speed ranging from 40 mm/s to 60 mm/s. The infill percentage was adjusted to 20% to balance strength and material usage, and a layer height of 0.2 mm was chosen to ensure good surface quality. Subsequently, a structure was designed and manufactured to serve as a support for the rotors in the triangular or Triframe configuration. Figure 7 illustrates the structure that forms the hydrokinetic array with the scale models of the turbines.



Figure 6. Scale models of Gorlov-type 3D-printed VAHTs.

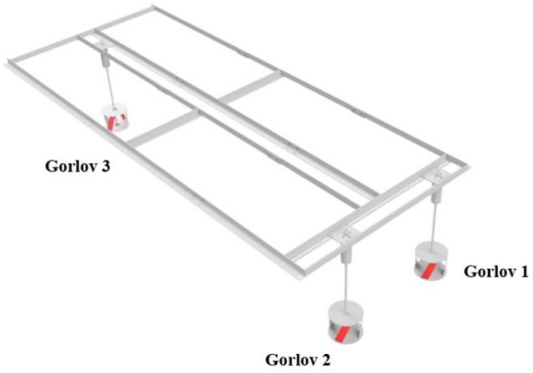


Figure 7. Structure of the scale model of the Gorlov-type VAHT array.

2.6.2. Experimentation with the Vertical-Axis Gorlov-Type Hydrokinetic Turbine Array

Once the scale models of the turbines and the structure shaping the hydrokinetic array were manufactured, the experimental setup was constructed to obtain the performance characteristic curves of each of the rotors operating together. The experimental testing system consisted of five components: the measurement system, the mounting plate, the bearing support, the shaft, and the rotor or turbine, as shown in Figure 8. The measurement system includes a torque sensor, a DC motor, mechanical couplings, and a support base. The torque sensor from FUTEK (TRS 605-FSH02052) has a measurement range of 0–1 Nm and is equipped with an encoder for measuring the rotational speed of the shaft. The second component of this system is a six VDC electric motor reducer, which primarily provides the electrical load on the turbine and acts as a brake. To measure the torque generated by the turbine at different rotational speeds (different TSR), a braking system was coupled to one end of the torque sensor. This system uses the six VDC motor reducer rotating in the opposite direction of the turbine, thereby generating a counteracting torque that reduces the turbine's rotation speed. The braking torque is adjusted by the amount of current flowing to the DC motor through pulse width modulation (PWM), which is achieved using a microcontroller (Arduino Nano) and a power coupling circuit in the developed system. When it is necessary to decrease (or increase) the turbine's rotation speed, the microcontroller increases (or decreases) the duty cycle of the PWM (i.e., modifies the pulse width), which increases (or decreases) the energy received by the motor, and consequently, the braking torque also increases (or decreases). The PWM system was

configured to increase the current supplied to the motor by 2% every 20 s, allowing the turbine to reach a steady-state condition after each load increase. Furthermore, this system was powered by a variable voltage source, on which a fixed voltage of 6 V and a current of 0.25 A (250 mA) were applied.

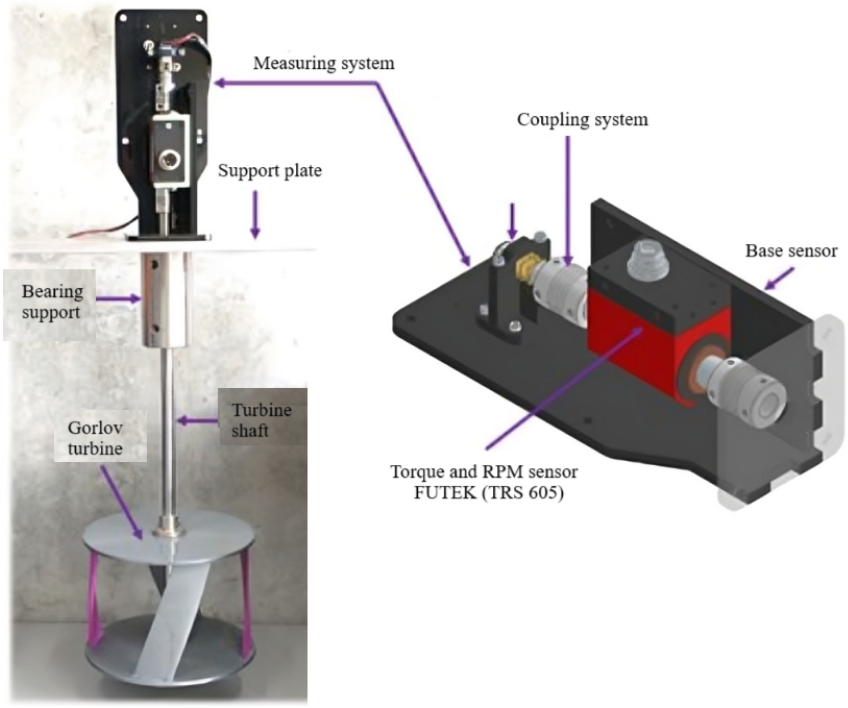


Figure 8. Assembly for experimental testing of Gorlov-type hydrokinetic turbine.

To acquire the data obtained from the sensor measurements, it was necessary to connect an additional portable reference device (Futek USB 520). This additional device collects real-time recorded data and transfers them to the computer through the sensit software interface, which is specially developed by the torque sensor manufacturer and the data acquisition device. The data from each measurement were exported for the generation of the Cp vs. TSR curve. For data reading and collection, a 20 min sampling period was configured in the program to capture all data corresponding to the load increase in the motor reducer.

Due to the overall dimensions of the hydrokinetic array in its optimal configuration, it was not possible to conduct experimental tests in hydraulic channels or a laboratory. The location where the experimentation of this research took place was in Colombia, Antioquia department, the municipality of El Retiro, in a section of the stream called "Tempranos" (latitude 6.0658496°; longitude −75.5020446°) at an elevation of 2145 m above sea level. The test section shown in Figure 9 had an approximate width of 6 m. Various measurements were taken across the width of the current to characterize the test section in terms of flow velocity and depth. The depth profile in this portion of the fluid flow was irregular, with values ranging from 0.3 to 0.65 m. However, the velocity profile could be considered homogeneous since the average fluid flow velocity was approximately 0.8 m/s, a value obtained at multiple points across the fluid current. Velocity measurements were taken using a Flow Watch propeller flow meter (FW450) with a resolution of ±0.01 m/s. The temperature in the test area ranged from a minimum of 13 °C to a maximum of 24 °C. The river is clear, with good visibility of the riverbed and no significant sediment transport affecting the measurements. The theoretical hydrokinetic power (P_{HKT}) of this location was 4.90 W. The theoretical power at the test site was 48.8% lower than the power from the computational simulations.



Figure 9. Experimental setup at the test site.

3. Results and Discussion

3.1. Numerical Simulation Results

The results of the numerical simulations for each of the nine experimental units are listed in Table 5. The maximum value for the response variable (P), defined as the sum of the power generated by each rotor, was achieved through experimental unit 7, resulting in a rotor separation distance relative to the diameter D of $16D$ in the direction of the fluid flow (X) and $4D$ across the flow (Y). The minimum value corresponded to experimental unit 3, resulting in a rotor separation distance relative to the diameter D of $1D$ in the direction of the fluid flow (X) and $2D$ across the flow (Y). Based on these initial observations, when designing hydrokinetic arrays that operate with vertical-axis Gorlov turbines, it is necessary to consider not only the downstream rotor spacing due to the formation of the fluid wake but also the lateral spacing between them, as the spacing across the river's flow appears to affect the array's power output to an equal or greater extent. To test or reject this claim, a statistical analysis of the numerical results was conducted.

Table 5. Numerical results for the different configurations of the hydrokinetic array.

Experimental Unit	$X(D)$	$Y(D)$	$P(W)$
1	16	2	2.3344
2	11	4	3.9656
3	11	2	2.1937
4	16	6	4.1906
5	11	6	3.3469
6	6	6	3.0375
7	16	4	4.3875
8	6	4	3.0656
9	6	2	1.9238

3.2. Statistical Analysis

Through statistical analysis, a mathematical model was established to predict the parameter combination that maximizes the total power generated by the hydrokinetic array (P). The open-source statistical software R-4.2.3 for Windows was used for this analysis, which facilitates data modeling and processing. Various types of functions can be employed to generate a regression model, including linear, quadratic, cubic functions, and some other special functions. However, in the field of turbine design, second-order response surfaces have been previously used [32,50]. A quadratic regression model was chosen to evaluate the individual, combined, and quadratic effects of the independent factors (X, Y) on the response variable (P). The generic equation representing the second-order model containing linear, combined, and quadratic terms is shown in Equation (6). Here, (P) represents the

response variable; β_0 is a constant value in the regression model, known as the intercept; β_1 and β_2 are the linear coefficients of the regression, corresponding to the individual effects of the factors; β_{12} is the combined coefficient, which explains the combined effects of the main factors on the response variable. Finally, β_{11} and β_{22} correspond to the quadratic coefficients [51].

$$P = \beta_0 + \beta_1 X + \beta_2 Y + \beta_{12} XY + \beta_{11} X_1^2 + \beta_{22} Y_2^2 \quad (6)$$

3.2.1. Developing the Regression Model

Based on the numerical simulation results reported in Table 5, the regression model was constructed using analysis of variance (ANOVA), which allows for distinguishing the contribution of each term involved in the generated regression models. To evaluate the ability of the regression model to describe the obtained numerical results, the following statistics were employed: model correlation coefficient R^2, model correlation coefficient adjusted for degrees of freedom R^2_{adjust}, and the model p-value. A significance level of $\alpha = 0.05$ was used for the statistical hypotheses. This value indicates a 5% risk of drawing incorrect conclusions from the results obtained through the application of the tests. The first statistical test established was the significance of the regression, which aims to determine the existence of a relationship between the independent variables (factors) and the response variable [38]. This led to the formulation of the hypothesis test: $H_0 : \beta_1 = \beta_2 = \ldots = \beta_k = 0$; $H_1 = \exists; \beta_j \neq 0$. Here, H_0 represents the null hypothesis, and H_1 signifies the rejection of H_0. Rejecting H_0 implies that at least one of the independent variables contributes significantly to the regression model. Three regression models were formulated, as shown in Table 6. It was observed that the independent variables (X, Y) contributed to the regression model, thus rejecting the null hypothesis H_0. However, not all terms of the generic second-order regression model were significant. According to the ANOVA for the generic second-order model, significance was only reported for the terms X, Y and Y^2 allowing for the modification of the generic second-order model by creating two additional models: the first retained only the significant terms, eliminating the interaction between X and Y, and the second retained only the significant terms while including the interaction between X and Y. The latter model proved to be highly significant and suitable for describing the relationship between the distances between turbines along and across the fluid flow and the total power generated by the hydrokinetic array. This choice was made because the modified second-order regression model with linear interaction had a p-value of 0.002, well below 0.05, and R^2_{adjust} of 0.9711, which was higher compared to the other regression models. Furthermore, the corresponding R^2 value for the modified second-order regression model with interactions showed that only 2.89% of the total variation in the experimental data could not be explained by the model.

Table 6. Statistical parameters of constructed regression models.

Regression Model	R^2	R^2_{adjust}	p-Value
Generic second-order model	97.11%	92.30%	0.01623
Modified second-order model with linear interaction	97.11%	94.22%	0.00246
Modified second-order model without linear interaction	94.96%	91.94%	0.00140

3.2.2. Analysis of ANOVA Results for the Chosen Regression Model

Table 7 displays the results yielded by the ANOVA for the modified second-order model with linear interaction, which relates the response variable to the independent variables.

Table 7. ANOVA results for the modified second-order regression model with linear interaction.

Term	Effect	Sum of Square	Degrees of Freedom	Mean Square	F-Ratio	*p*-Value
Model		6.2346	4	1.5586	33.58	0.00246
X	0.02194	1.3878	1	1.3878	29.897	0.00544
Y	2.07624	2.8333	1	2.8333	61.038	0.00145
Y^2	−0.24210	1.8757	1	1.8757	40.407	0.00314
XY	0.01856	0.1378	1	0.1378	2.969	0.15996
Error		0.1857	4	0.0465		

According to the ANOVA results, it is observed that the variable associated with the spacing between rotors across the fluid flow (Y) has a greater impact on the response variable, considering the *p*-value, compared to the other terms in the model. This result is consistent with the studies reported by [27,29], which suggest that for the design of hydrokinetic arrays or farms, one should consider not only the spacing between rotors downstream but also the lateral spacing between them. The mathematical expression describing the response of the total power of the hydrokinetic array (P) to variations in distances along the fluid flow direction (X) and across it (Y) is given by Equation (7).

$$P = -1.68310 + 0.02194X + 2.07624Y + 0.01856XY - 0.24210Y^2 \quad (7)$$

3.2.3. Assumption Verification

For the specific case of the constructed regression model, the following analyses were conducted: normality of residuals, no autocorrelation of residuals (independence), and constant variance of residuals (homoscedasticity). Normality can be assessed graphically through the construction of a frequency distribution and a normal probability plot [52], as shown in Figure 10. However, it is not clear whether the normality assumption is accepted. Therefore, numerical tests described in Table 8 were performed to confirm the normality assumption, with the Shapiro–Wilk test being the most relevant test for all types of data and sample sizes compared to other normality tests [53,54]. There is no evidence to reject the normality assumption, as the *p*-value assigned to the entire set of normality tests conducted was greater than 0.05.

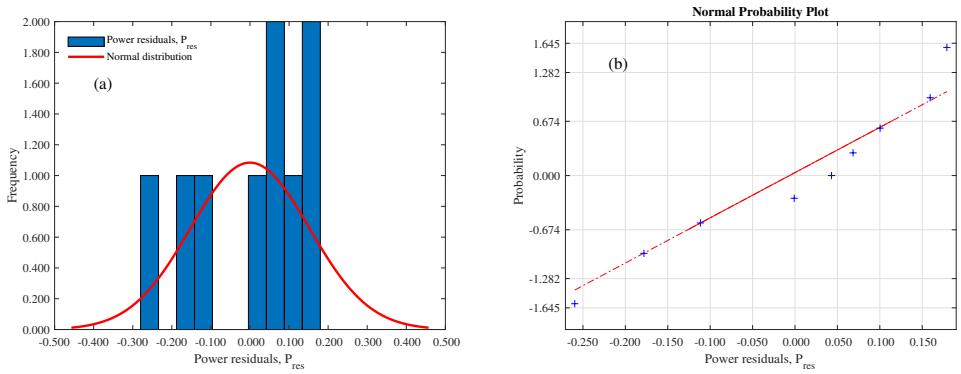


Figure 10. Distribution analysis: frequency distribution and normal probability plot. (**a**) Frequency distribution. (**b**) Normal probability plot.

Table 8. Normality tests for the response variable.

Normality Test	*p*-Value
Shapiro–Wilk test	0.5585
KS limiting form	0.9636
KS Stephens modification	0.1500

Table 8. *Cont.*

Normality Test	*p*-Value
Anderson–Darling test	0.5431
Cramer–von Mises test	0.5212
Shapiro–Francia test	0.6303
KS Marsaglia method	0.9299
Jarque–Bera test	0.6766
D'Agostino and Pearson test	0.5983
KS Lilliefors modification	0.2000

To check for independence in the residuals, the Durbin–Watson test was used, which evaluates the presence of residual autocorrelation based on the regression model evaluation [52]. The test resulted in a *p*-value of 0.2899; hence, the assumption of independence, meaning no autocorrelation of the residuals, could not be rejected. Additionally, homoscedasticity was assessed using the Breusch–Pagan test, which informs about the dependence of error variance on the values of the independent variable. With a *p*-value of 0.1607, it can be confirmed that homoscedasticity exists. Therefore, the second-order regression model modified with linear interaction constructed through a 3^k factorial design can be used to predict the response to any combination of the investigated variables in the experimental domain. Furthermore, the regression model can be used to achieve higher hydrokinetic array power, valid only within the experimental range. The following Table 9 presents a comparison between the results obtained through simulation and the results of the regression model, along with the percentage of error.

Table 9. Comparison of numerical results obtained for the total power of the array with those predicted by the selected regression model.

Experimental Unit	$X(D)$	$Y(D)$	CFD Result $P(W)$	Predicted Result $P(W)$	% Error
1	16	2	2.3344	2.4459	4.77
2	11	4	3.9656	3.8062	4.01
3	11	2	2.1937	2.1506	1.96
4	16	6	4.1906	4.1915	0.02
5	11	6	3.3469	3.5250	5.32
6	6	6	3.0375	2.8585	5.89
7	16	4	4.3875	4.2871	2.28
8	6	4	3.0656	3.3253	8.47
9	6	2	1.9238	1.8553	3.55

3.3. Determination of the Optimal Point for the Hydrokinetic Array

Defining the values of the factors involved in the experimental design plays a crucial role, as it allows for determining the combination of the studied factors or treatment that, in this case, maximizes the value of the response variable. This is the final step to completing the optimization procedure with the response surface methodology. In the case of optimization through the response surface methodology, the candidate optimal point (commonly referred to as the stationary point) is, by definition, the point where a plane tangent to the response surface has a slope equal to 0 [52]. To find the best configuration for all the factors, Statgraphics Centurion XVII software was used. The optimization process aimed to maximize the response variable (P) and found that the combination of values for the independent variables that achieved this purpose was $15.9672D$ for X and $4.15719D$ for Y. Figure 11 provides the response surface obtained from the optimization process described in this work. It is evident that there is an inflection point on the surface, and this is where the highest values for the power of the hydrokinetic array are achieved.

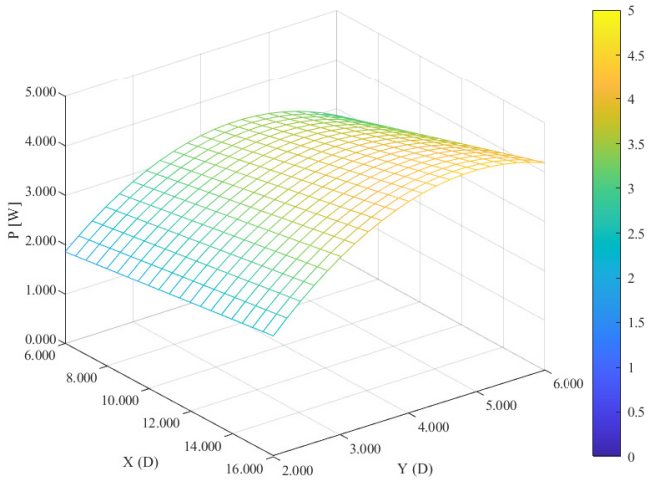


Figure 11. The response surface for the response variable P as a function of the independent variables.

3.4. Validation of Treatments with Optimal Values

With the values of the optimum point, a new numerical simulation of the vertical-axis Gorlov hydrokinetic turbine array was conducted. Table 10 presents the obtained values for the total power generated by the optimized hydrokinetic array configuration and the values obtained for experimental unit 7, which reported the highest power (P) in the experimental matrix detailed in Table 9.

From Table 10, it was established that the optimal configuration of the hydrokinetic array achieved an approximate total power of 4.4 W. This represents an increase of 2.809% compared to the experimental unit that reported the highest total power. Based on these results, it can be concluded that the optimization of the mathematical model describing the total power response of the hydrokinetic array (P) for variations in distances along the fluid flow direction (X) and width (Y) was successful. The optimal values for the mathematical model yielded higher total power results than all the experimentally simulated units.

Table 10. Comparison of the total power generated for the optimized hydrokinetic array and the best experimental unit.

Experimental Unit	$X(D)$	$Y(D)$	$P(W)$	Rate of Increase (%)
7	16	4	4.28714	-
Optimized arrangement	15.9672	4.15719	4.4076	2.809

Furthermore, the optimization process was complemented with a C_p vs. TSR graph for the optimal configuration of the hydrokinetic array, as shown in Figure 12. It is noticeable that the turbines are aligned in parallel and interact initially with the fluid flow, resulting in similar efficiencies. However, the downstream turbine produces more power from the fluid flow, registering higher velocity peaks and slight increases in torque magnitude, indicating higher efficiency. This can be justified by the operating principle based on the lift force for Gorlov-type vertical-axis hydrokinetic turbines. These turbines do not use all the blades to generate turbine rotation. Instead, this task is distributed, leaving at least one blade free at each moment of rotation. The free blade does not contribute to lift but produces drag force. The blades responsible for rotation generate positive torque. However, the free blade exerts minimal negative torque on the turbine rotor. This is because the free blade rotates against the water flow. Therefore, the output power of the Gorlov-type vertical-axis hydrokinetic turbines improves by blocking the flow on the free blade. Considering this, the fluid wakes shed by the turbines in the first row of the hydrokinetic array play a role in generating a low-energy region, blocking the flow towards the free blade and mitigating the negative

torque generated by it, favoring the turbine by increasing its revolution rate and slightly increasing the torque. However, it was observed that this phenomenon only occurs at the end of the fluid wakes generated by the first row of rotors, meaning when the fluid flow tends to regain the turbulence regime that it carried upstream of the first row of rotors. Otherwise, with higher turbulence intensities in the fluid wakes, only a blocking effect is achieved, preventing the rotation of the rotors located downstream of the first row, which are also part of the hydrokinetic array [12,15].

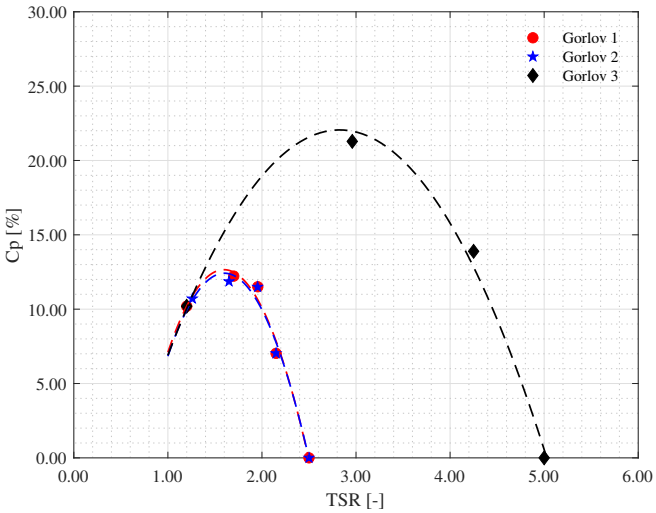


Figure 12. Numerical C_p vs. TSR curve of the three turbines that make up the optimized hydrokinetic array.

3.5. Experimental Results

Experimental tests were conducted with the model in its optimized configuration. Regarding the total power captured by the hydrokinetic array, calculated as the sum of the maximum power of each rotor, a power close to 3.4 W was obtained. This slightly differs from the power reported in the numerical simulations for the optimized hydrokinetic array, which was close to 4.4 W. The difference in power can be attributed to the flow velocities during testing: the simulations were conducted at a flow speed of 1 m/s, while the experimental tests were performed at a lower flow speed of 0.8 m/s.

The efficiency of the hydrokinetic array in the simulations can be calculated by dividing the power captured (4.4 W) by the theoretical available power for the array, which is three times the theoretical power of a single turbine (9.57 W $\times$ 3 = 28.71 W). This results in an efficiency of approximately 15.3%. For the experimental tests, the efficiency is determined by dividing the power captured (3.4 W) by the theoretical available power for the array (4.90 W $\times$ 3 = 14.70 W), yielding about 23.1%. These efficiency calculations highlight that while the array showed lower efficiency in simulations compared to the theoretical values, the experimental results demonstrated a higher relative efficiency considering the reduced available power.

The differences observed between the experimental results and the numerical simulations can be attributed to several factors that were not considered in the simulations. These include the physical components, such as the effects of shafts and bearings, as well as the surface quality of the turbine blades. Additionally, in the natural testing environment, several variables introduce uncertainty, such as variations in fluid flow rate, turbulence levels, and mechanical friction. Furthermore, the presence of sediments like sticks, leaves, and sand interacting with the rotors could have influenced the results. Despite these challenges, the efficiency values obtained for each rotor are consistent with experimental studies of VAHTs with helical blades [5,15,55,56].

Based on the experimental data obtained for the optimized hydrokinetic array, characteristic curves were obtained for each of the three turbines that make up the hydrokinetic

array, in terms of C_p vs. TSR, as summarized in Figure 13. It is noteworthy that the hydrodynamic behavior of the three rotors comprising the hydrokinetic array partially retains the shape and trend reported by the numerical simulations, especially for the two rotors located in the front row of the hydrokinetic array. The rotor named Gorlov 3 exhibited the greatest variations and the highest performance peaks. Through experimentation, it was observed that the wakes from the turbines in the first row did not alter the rotational speed of the Gorlov 3 rotor but did increase the torque, resulting in slightly higher power. This also aligns with the fluid dynamic analysis described in the C_p vs. TSR graph obtained through numerical simulation for the optimized configuration of the hydrokinetic array, where the rear rotor had the highest performance.

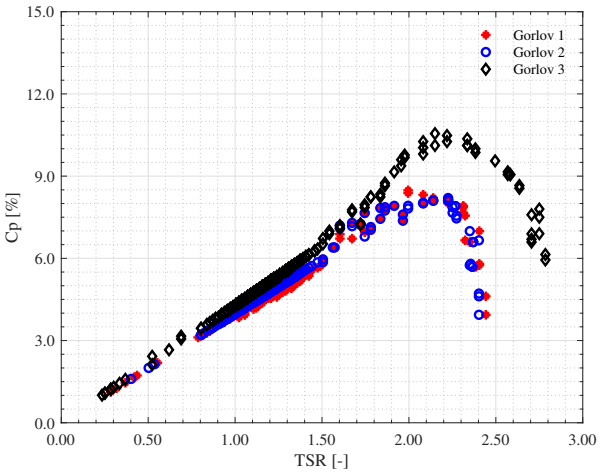


Figure 13. Experimental C_p vs. TSR curve for the three turbines that make up the hydrokinetic array.

4. Conclusions

The theoretical considerations for designing and developing an energy generation system using Gorlov vertical-axis hydrokinetic turbines (VAHTs) in a hydrokinetic array or farm configuration were thoroughly reviewed. The main conclusions were the following:

- The experimental design employed was a 3^k factorial design, analyzing two factors at three levels of variation, resulting in nine treatments or experimental units. These nine treatments were numerically simulated using ANSYS software, specifically within the ANSYS-Fluent environment, utilizing the 6-DOF tool to analyze the fluid dynamic behavior of three Gorlov-type hydrokinetic turbines in a Triframe configuration.
- The optimization process was conducted using response surface methodology (RSM), with a detailed validation of treatments that yielded optimal values. The separation distance between rotors, both along (X) and across (Y) the fluid flow direction, significantly impacted the total power generated by the hydrokinetic array (P).
- The optimal values for these factors, expressed in terms of the turbine diameter D, were found to be $15.9672D$ for X and $4.15719D$ for Y, resulting in a power output of 4.4076 W, representing a 2.809% increase compared to experimental unit 7, which had reported the highest power output in the initial experimental matrix.
- The method of 3D printing was utilized to create three scale models of the Gorlov VAHTs used in the hydrokinetic array. A support structure was also designed to maintain the three rotors in their optimal configuration. The experimental setup was conducted in the Tempranos stream, near Retiro, Antioquia, due to the array's size. The installation included the rotors, support structure, and measurement instruments to evaluate the system's performance in terms of C_p and TSR.

Numerical and experimental approaches are essential for developing devices and systems that harness renewable resources. Numerical simulation, combined with response surface methodology (RSM), offers an efficient alternative for optimization processes that

would otherwise be prohibitively expensive due to the multitude of resulting treatments. However, numerical simulations must be validated by experimental results to account for and quantify the negative effects of variables not included in the numerical models due to time constraints and high computational costs.

Future research on Gorlov vertical-axis hydrokinetic turbines (VAHTs) should start with investigating various array configurations and rotor arrangements beyond the current Triframe setup to further optimize power generation and spatial efficiency. To validate these designs in real-world scenarios, field tests of larger-scale hydrokinetic arrays in diverse environmental conditions are essential. Additionally, integrating VAHTs with energy storage systems could help manage energy production and ensure a consistent energy supply. It is also important to study the effects of varying environmental conditions, such as water flow rates, sediment loads, and seasonal variations, on the performance and longevity of VAHTs. Improvements in measurement and data collection methods are also needed to better assess rotor design parameters, including variations in blade shape, material, and construction methods. Lastly, implementing long-term monitoring programs will help study the reliability and performance of VAHTs over extended periods, identifying potential areas for further improvement.

Author Contributions: Writing—original draft preparation, A.C. and L.V.; methodology, A.C., L.V., E.C. and A.R.-C.; formal analysis, L.V., A.R.-C. and E.C.; experimental setup, L.V., A.C., A.R.-C. and E.C.; writing—review and editing, A.R.-C. and E.C.; funding acquisition, A.R.-C. and E.C.; project administration, A.R.-C. and E.C.; supervision, E.C. All authors have read and agreed to the published version of the manuscript.

Funding: This research received no external funding.

Data Availability Statement: The data used for the preparation of the manuscript and discussion of results are contained within.

Acknowledgments: The authors gratefully acknowledge the support provided by the Colombian Ministry of Science, Technology, and Innovation "MinCiencias" through "Patrimonio Autónomo Fondo Nacional de Financiamiento para la Ciencia, la Tecnología y la Innovación, Francisco José de Caldas" Perseo Alliance, Contract No. 112721-392-2023.

Conflicts of Interest: The authors declare no conflicts of interest.

References

1. Scheffran, J.; Felkers, M.; Froese, R. Economic growth and the global energy demand. In *Green Energy to Sustainability: Strategies for Global Industries*; John Wiley & Sons: Hoboken, NJ, USA, 2020; pp. 1–44.
2. Kanwal, S.; Mehran, M.T.; Hassan, M.; Anwar, M.; Naqvi, S.R.; Khoja, A.H. An integrated future approach for the energy security of Pakistan: Replacement of fossil fuels with syngas for better environment and socio-economic development. *Renew. Sustain. Energy Rev.* **2022**, *156*, 111978. [CrossRef]
3. Yoro, K.O.; Daramola, M.O. CO2 emission sources, greenhouse gases, and the global warming effect. In *Advances in Carbon Capture*; Elsevier: Amsterdam, The Netherlands, 2020; pp. 3–28.
4. Gorlov, A. Hydrogen as an activating fuel for a tidal power plant. *Int. J. Hydrogen Energy* **1981**, *6*, 243–253. [CrossRef]
5. Kamal, M.M.; Saini, R. A review on modifications and performance assessment techniques in cross-flow hydrokinetic system. *Sustain. Energy Technol. Assess.* **2022**, *51*, 101933. [CrossRef]
6. Song, K.; Wang, W.Q.; Yan, Y. Numerical and experimental analysis of a diffuser-augmented micro-hydro turbine. *Ocean Eng.* **2019**, *171*, 590–602. [CrossRef]
7. Khan, M.; Bhuyan, G.; Iqbal, M.; Quaicoe, J. Hydrokinetic energy conversion systems and assessment of horizontal and vertical axis turbines for river and tidal applications: A technology status review. *Appl. Energy* **2009**, *86*, 1823–1835. [CrossRef]
8. Flórez, R.O. *Pequeñas Centrales Hidroeléctricas*; Ediciones de la U: Bogotá, Colombia, 2011.
9. Silva dos Santos, I.F.; Ramirez Camacho, R.G.; Tiago Filho, G.L.; Barkett Botan, A.C.; Vinent, B.A. Energy potential and economic analysis of hydrokinetic turbines implementation in rivers: An approach using numerical predictions (CFD) and experimental data. *Renew. Energy* **2019**, *143*, 648–662. [CrossRef]
10. Lalander, E.; Leijon, M. Numerical modeling of a river site for in-stream energy converters. In Proceedings of the EWTEC09, Uppsala, Sweden, 7–10 September 2009.
11. Saini, G.; Saini, R.P. A review on technology, configurations, and performance of cross-flow hydrokinetic turbines. *Int. J. Energy Res.* **2019**, *43*, 6639–6679. [CrossRef]

12. Patel, V.; Eldho, T.; Prabhu, S. Experimental investigations on Darrieus straight blade turbine for tidal current application and parametric optimization for hydro farm arrangement. *Int. J. Mar. Energy* **2017**, *17*, 110–135. [CrossRef]
13. dos Santos, I.F.S.; Camacho, R.G.R.; Tiago Filho, G.L. Study of the wake characteristics and turbines configuration of a hydrokinetic farm in an Amazonian river using experimental data and CFD tools. *J. Clean. Prod.* **2021**, *299*, 126881. [CrossRef]
14. Zhou, D.; Deng, Z.D. Ultra-low-head hydroelectric technology: A review. *Renew. Sustain. Energy Rev.* **2017**, *78*, 23–30. [CrossRef]
15. Nag, A.K.; Sarkar, S. Techno-economic analysis of a micro-hydropower plant consists of hydrokinetic turbines arranged in different array formations for rural power supply. *Renew. Energy* **2021**, *179*, 475–487. [CrossRef]
16. Sood, M.; Singal, S.K. Development of hydrokinetic energy technology: A review. *Int. J. Energy Res.* **2019**, *43*, 5552–5571. [CrossRef]
17. Cacciali, L.; Battisti, L.; Dell'Anna, S. Multi-array design for hydrokinetic turbines in hydropower canals. *Energies* **2023**, *16*, 2279. [CrossRef]
18. Okulov, V.; Naumov, I.; Kabardin, I.; Litvinov, I.; Markovich, D.; Mikkelsen, R.; Sørensen, J.; Alekseenko, S.; Wood, D. Experiments on line arrays of horizontal-axis hydroturbines. *Renew. Energy* **2021**, *163*, 15–21. [CrossRef]
19. Riglin, J.; Daskiran, C.; Jonas, J.; Schleicher, W.C.; Oztekin, A. Hydrokinetic turbine array characteristics for river applications and spatially restricted flows. *Renew. Energy* **2016**, *97*, 274–283. [CrossRef]
20. Khan, M.; Iqbal, M.; Quaicoe, J. Design considerations of a straight bladed Darrieus rotor for river current turbines. In Proceedings of the 2006 IEEE International Symposium on Industrial Electronics, Montréal, QC, Canada, 9–13 July 2006; IEEE: Piscataway, NJ, USA, 2006; Volume 3, pp. 1750–1755.
21. Gunawan, B.; Neary, V.S.; Mortensen, J.; Roberts, J.D. *Assessing and Testing Hydrokinetic Turbine Performance and Effects on Open Channel Hydrodynamics: An Irrigation Canal Case Study*; Technical Report; Sandia National Lab. (SNL-NM): Albuquerque, NM, USA, 2017.
22. Gorban', A.N.; Gorlov, A.M.; Silantyev, V.M. Limits of the turbine efficiency for free fluid flow. *J. Energy Resour. Technol.* **2001**, *123*, 311–317. [CrossRef]
23. Vennell, R.; Funke, S.W.; Draper, S.; Stevens, C.; Divett, T. Designing large arrays of tidal turbines: A synthesis and review. *Renew. Sustain. Energy Rev.* **2015**, *41*, 454–472. [CrossRef]
24. Malki, R.; Masters, I.; Williams, A.J.; Croft, T.N. Planning tidal stream turbine array layouts using a coupled blade element momentum–computational fluid dynamics model. *Renew. Energy* **2014**, *63*, 46–54. [CrossRef]
25. Olczak, A.; Stallard, T.; Feng, T.; Stansby, P. Comparison of a RANS blade element model for tidal turbine arrays with laboratory scale measurements of wake velocity and rotor thrust. *J. Fluids Struct.* **2016**, *64*, 87–106. [CrossRef]
26. Chawdhary, S.; Hill, C.; Yang, X.; Guala, M.; Corren, D.; Colby, J.; Sotiropoulos, F. Wake characteristics of a TriFrame of axial-flow hydrokinetic turbines. *Renew. Energy* **2017**, *109*, 332–345. [CrossRef]
27. González-Gorbeña, E.; Qassim, R.Y.; Rosman, P.C. Optimisation of hydrokinetic turbine array layouts via surrogate modelling. *Renew. Energy* **2016**, *93*, 45–57. [CrossRef]
28. Birjandi, A.H.; Bibeau, E.L. Frequency analysis of the power output for a vertical axis marine turbine operating in the wake. *Ocean Eng.* **2016**, *127*, 325–334. [CrossRef]
29. Nago, V.G.; dos Santos, I.F.S.; Gbedjinou, M.J.; Mensah, J.H.R.; Tiago Filho, G.L.; Camacho, R.G.R.; Barros, R.M. A literature review on wake dissipation length of hydrokinetic turbines as a guide for turbine array configuration. *Ocean Eng.* **2022**, *259*, 111863. [CrossRef]
30. Gaiser, K.; Erickson, P.; Stroeve, P.; Delplanque, J.P. An experimental investigation of design parameters for pico-hydro Turgo turbines using a response surface methodology. *Renew. Energy* **2016**, *85*, 406–418. [CrossRef]
31. Tian, W.; Mao, Z.; Ding, H. Design, test and numerical simulation of a low-speed horizontal axis hydrokinetic turbine. *Int. J. Nav. Archit. Ocean Eng.* **2018**, *10*, 782–793. [CrossRef]
32. Bouvant, M.; Betancour, J.; Velásquez, L.; Rubio-Clemente, A.; Chica, E. Design optimization of an Archimedes screw turbine for hydrokinetic applications using the response surface methodology. *Renew. Energy* **2021**, *172*, 941–954. [CrossRef]
33. de la Vara Salazar, R. *Análisis y Diseño de Experimentos*; McGraw-Hill: New York, NY, USA, 2004.
34. Khan, Z.U.; Ali, Z.; Uddin, E. Performance enhancement of vertical axis hydrokinetic turbine using novel blade profile. *Renew. Energy* **2022**, *188*, 801–818. [CrossRef]
35. Rezaeiha, A.; Kalkman, I.; Blocken, B. CFD simulation of a vertical axis wind turbine operating at a moderate tip speed ratio: Guidelines for minimum domain size and azimuthal increment. *Renew. Energy* **2017**, *107*, 373–385. [CrossRef]
36. Tu, J.; Yeoh, G.H.; Liu, C.; Tao, Y. *Computational Fluid Dynamics: A Practical Approach*; Elsevier: Amsterdam, The Netherlands, 2023.
37. Sosnowski, M.; Krzywanski, J.; Grabowska, K.; Gnatowska, R. Polyhedral meshing in numerical analysis of conjugate heat transfer. In *EPJ Web of Conferences*; EDP Sciences: Les Ulis, France, 2018; Volume 180, p. 02096.
38. Fluent, A. *Ansys Fluent 12.0 Theory Guide*; Ansys Inc.: Canonsburg, PA, USA, 2009.
39. Antonini, E.G.; Romero, D.A.; Amon, C.H. Analysis and modifications of turbulence models for wind turbine wake simulations in atmospheric boundary layers. *J. Sol. Energy Eng.* **2018**, *140*, 031007. [CrossRef]
40. Liu, Y.; Yang, Y.; Zhang, H.; Zhang, L. Computational fluid dynamics prediction of the dynamic behavior of autonomous underwater vehicles. *IEEE J. Ocean. Eng.* **2019**, *45*, 724–739. [CrossRef]
41. Prakoso, A.P.; Warjito, W.; Siswantara, A.I.; Budiarso, B.; Adanta, D. Comparison between 6-dof udf and moving mesh approaches in cfd methods for predicting cross-flow picohydro turbine performance. *CFD Lett.* **2019**, *11*, 86–96.

42. Messmer, T.; Brigden, C.; Peinke, J.; Hölling, M. A six degree-of-freedom set-up for wind tunnel testing of floating wind turbines. *J. Phys. Conf. Ser.* **2022**, *2265*, 042015. [CrossRef]
43. Betancour, J.; Velásquez, L.; Rubio Clemente, A.; Chica, E. Performance simulation of water turbines by using 6-DoF UDF and sliding mesh methods. *J. Appl. Res. Technol.* **2023**, *21*, 181–195.
44. Keough, R.; Mullaley, V.; Sinclair, H.; Walsh, G.; Hinchey, M. *Design, Fabrication and Testing of a Water Current Energy Device*; Project Report; Memorial University of Newfoundland: St. John's, NL, Canada, 2014.
45. Frank, M.W. *Mecánica de Fluidos*, 6th ed.; SAU [Consulta: 17/12/2015]; McGraw-Hill Interamericana de España: New York, NY, USA, 2015.
46. Roache, P.J. *Verification and Validation in Computational Science and Engineering*; Hermosa: Albuquerque, NM, USA, 1998; Volume 895.
47. Lee, J.; Kim, Y.; Khosronejad, A.; Kang, S. Experimental study of the wake characteristics of an axial flow hydrokinetic turbine at different tip speed ratios. *Ocean Eng.* **2020**, *196*, 106777. [CrossRef]
48. Ebel, E.; Sinnemann, T. Fabrication of FDM 3D objects with ABS and PLA and determination of their mechanical properties. *RTe J.* **2014**, *11*, 1–11.
49. Bade, L.; Hackney, P.; Shyha, I.; Birkett, M. Investigation into the development of an additive manufacturing technique for the production of fibre composite products. *Procedia Eng.* **2015**, *132*, 86–93. [CrossRef]
50. Gallego, E.; Rubio-Clemente, A.; Pineda, J.; Velásquez, L.; Chica, E. Experimental analysis on the performance of a pico-hydro Turgo turbine. *J. King Saud Univ.-Eng. Sci.* **2021**, *33*, 266–275. [CrossRef]
51. Walpole, R.E.; Myers, R.M.; Myers, S.L.; Ye, K. *Probabilidad y Estadística para Ingeniería y Ciencias*; Pearson Educación: Naucalpan de Juárez, Mexico, 1992.
52. Myers, R.H.; Montgomery, D.C.; Anderson-Cook, C.M. *Response Surface Methodology: Process and Product Optimization Using Designed Experiments*; John Wiley & Sons: Hoboken, NJ, USA, 2016.
53. Razali, N.M.; Wah, Y.B. Power comparisons of shapiro-wilk, kolmogorov-smirnov, lilliefors and anderson-darling tests. *J. Stat. Model. Anal.* **2011**, *2*, 21–33.
54. Yap, B.W.; Sim, C.H. Comparisons of various types of normality tests. *J. Stat. Comput. Simul.* **2011**, *81*, 2141–2155. [CrossRef]
55. Mohamed, M. Performance investigation of H-rotor Darrieus turbine with new airfoil shapes. *Energy* **2012**, *47*, 522–530. [CrossRef]
56. Takao, M.; Kuma, H.; Maeda, T.; Kamada, Y.; Oki, M.; Minoda, A. A straight-bladed vertical axis wind turbine with a directed guide vane row—Effect of guide vane geometry on the performance. *J. Therm. Sci.* **2009**, *18*, 54–57. [CrossRef]

Disclaimer/Publisher's Note: The statements, opinions and data contained in all publications are solely those of the individual author(s) and contributor(s) and not of MDPI and/or the editor(s). MDPI and/or the editor(s) disclaim responsibility for any injury to people or property resulting from any ideas, methods, instructions or products referred to in the content.